

THE RESOLVED OUTER POPULATION OF NGC6822 WITH WFPC2

J. B. Hutchings¹

Dominion Astrophysical Observatory, National Research Council of Canada,
Victoria, B.C. V8X 4M6, Canada

B. Cavanagh

Department of Physics and Astronomy, University of Victoria, B.C. V8W 3P6, Canada

L. Bianchi¹

Center for Astrophysical Sciences, Dept of Physics and Astronomy, Johns Hopkins
University, Baltimore, MD 21218

ABSTRACT

We present F336W (*U*), F439W (*B*), F555W (*V*), and F675W (*R*) Wide Field Planetary Camera 2 (WFPC2) photometry of two outer regions of the Local Group dwarf irregular galaxy NGC6822. The NE region is ~ 13 arcmin from the galaxy centre, while the W region lies 10 arcmin out, and within the wispy low surface brightness outer regions of the galaxy. The fields are not crowded and contain few NGC 6822 stars. We discuss errors and uncertainties and find that the W region contains a main sequence that extends to stars of about $2 M_{\odot}$, with an age of about 200 Myr. The NE region has no main sequence or stars younger than 1 Gyr, but does contain some luminous red stars that are not matched in the W field. These stars are not clumped in the field. The results suggest that the W region may be a trace of a tidal event that triggered the current star-formation in this isolated galaxy.

Subject headings: Galaxies: stellar content, galaxies: local group

¹Observer with the NASA/ESA *Hubble Space Telescope* at the Space Telescope Science Institute, which is operated by the Association of Universities for Research in Astronomy, Inc., under NASA contract NAS 5-26555.

1. INTRODUCTION

The Local Group dwarf irregular galaxy NGC6822 was the first extra-Galactic object to have its distance measured by Hubble (1925) using the period-luminosity relation of Cepheids. Since these original observations, NGC6822 has been studied in varying degrees of detail. This galaxy has been classified as a type Ir IV-V by van den Bergh (1968), which is a similar classification as the Small Magellanic Cloud. The distance modulus has been more accurately determined since Hubble’s initial calculation of 21.65 (corresponding to a distance of 214 kpc); current values are close to 23.5, which is a distance of 500 kpc (McAlary et al 1983). NGC6822 has optical dimensions of $6' \times 11'$, which corresponds to a size of 1.7×3.2 kpc at a distance of 500 kpc. Galaxy parameters are given in Table 1. Roberts (1972) showed that the optical core is embedded in a large gaseous envelope with dimensions $42' \times 89'$ (12.2×25.9 kpc at 500 kpc). Inspection of the DSS image of the galaxy shows that the W side has extensive faint streaky light that is not present on the E side. It is of interest to know whether this arises from stars belonging to the galaxy. If so, they may be the remnants of a tidal event that has triggered the current star-formation activity in this apparently isolated galaxy.

Many of the previous photometric surveys of NGC6822 have studied either specific objects within the galaxy, or the galaxy as a whole. NGC6822 has many H II regions, most of which lie along the northern edge of the galaxy, and which have been studied extensively. OB associations in the galaxy have also been studied (Massey et al 1995). Stars found in these regions are mostly young, high-luminosity stars. Very few studies have examined the outer regions of NGC6822 to probe its stellar population. For example, Massey’s (1998) control field is closer to the galaxy than the fields of this study. A ‘halo’ population was found in the Local Group Im IV-V dwarf irregular galaxy WLM by Minniti and Zijlstra (1996), so a similar population in NGC6822 seems likely.

2. OBSERVATIONS

Observations were obtained with the Wide Field Planetary Camera 2 (WFPC2) on the *Hubble Space Telescope* (*HST*) as coordinated parallels with spectroscopy of OB stars in selected associations (program GO6567). The spacecraft roll angles were specified to maximise overlap in two areas to the E and W of the main galaxy body, using five different filters. For each pointing we obtained exposures with two different filters, in order to obtain the maximum filter coverage for the overlapping areas, and providing one color for each complete WFPC2 field. Details are shown in Table 2.

Data sets 1 & 2 (the ‘East’ region) overlap some 13 arcsec NE of the galaxy centre, and data sets 3, 4, & 5 (the ‘West’ region) overlap some 10 arcsec W of the galaxy centre. This enables photometry in four wavelength bands for a subset of resolved stars. Figures 1 & 2 show the positions of the fields on the sky.

The data were reduced using profile-fitting photometry, and examined for individual pointings, and then for the overlap regions of nearby pointings. The W sets (3, 4, 5) lie within the streaky extended flux of the galaxy while the E region (1, 2) appear to lie clear of any galaxy light seen in the DSS. Aperture corrections were made to determine correct zeropoints and offsets, followed by foreground star decontamination and de-reddening corrections, as described in the sections following.

3. PHOTOMETRY

3.1. Individual Sets

All individual sets of WFPC2 images were reduced using DAOPHOT (Stetson 1987) under IRAF² using the following technique:

(1) the FIND routine was used to find starlike objects exceeding the local background by four standard deviations in the images observed at the higher wavelength (i.e., for data set 1, the observation with the F555W filter was used);

(2) the PHOT routine was used to determine initial estimates of the magnitude of each starlike object by aperture photometry;

(3) a point-spread function was determined by manually selecting stars in each frame, then using a Moffat function with $\beta=1.5$ to fit to the stellar images to a radius of 10 pixels;

(4) the ALLSTAR routine was used to obtain profile-fitting magnitudes for the stars in the frame;

(5) aperture photometry of the images at lower wavelength was performed using the coordinate list obtained from the higher wavelength observation, using the PHOT routine; and

(6) the ALLSTAR routine was used to obtain profile-fitting magnitudes for stars in the

²IRAF is distributed by the National Optical Astronomy Observatories, which are operated by the Association of Universities for Research in Astronomy, Inc., under cooperative agreement with the National Science Foundation.

frame observed at the lower wavelength using the PSF obtained for the higher wavelength observation.

The sky levels were determined from simple statistics on the entire images, and checked against the final star-subtracted images. The fields are not crowded so that the sky level was always well determined and not a source of photometric error. Once magnitudes for each wavelength were obtained, the resulting tables were merged according to star ID number; if a starlike object was detected and measured in both wavelengths, then there is a good chance that this object is a star. Chance alignments with cosmic rays were eliminated by rejecting objects with a *CHI* fitting parameter greater than 1.5 in the lower wavelength images. A random inspection of objects thus rejected showed that they were indeed cosmic rays and not stars. This threshold also rejects stars that have saturated the WFPC2 detectors and would have otherwise been rejected.

ALLSTAR estimates measuring errors for all objects. These reach a mean of 0.2 mag at the following magnitudes (and filters): 24.7 (F675W), 24.5 (F555W), 23.2 (F439W), 22.3 (F336W). Objects with errors in the higher wavelength band greater than 0.25 mag were also rejected.

3.2. Overlapping Sets

The overlapping sets were reduced by the method described above, with some modifications. First, images were aligned using reference stars in each overlapping image. To ensure the photometry does not change when images are shifted and rotated, aperture photometry was done on the reference stars in the pre- and post-alignment images; results agreed to within 0.02 magnitudes, below the average errors obtained from ALLSTAR. After the images were aligned, magnitudes for all stars were obtained using the above techniques. Once magnitudes were determined, objects appearing at the same location (within a 3-pixel fitting radius) in all four wavelengths were kept. Again, there is a chance of alignment with cosmic rays, so objects with a *CHI* fitting parameter greater than 1.5 were rejected. Objects with errors in the higher wavelength band greater than 0.25 mag were also rejected.

3.3. Aperture Corrections and Errors

Because the ALLSTAR profile-fitting routine uses, as a basis for its magnitudes, a preliminary crude estimate of the magnitude obtained using a small synthetic diaphragm, chosen to avoid contamination from neighbouring stars, the magnitudes it obtains will be

offset from the true instrumental magnitudes by some amount. This offset was determined by performing aperture photometry on uncrowded stars, primarily those stars used to determine the PSF in step (3), above. For observations at lower wavelengths (for which no PSF was determined), uncrowded stars were chosen by hand. In addition, because the zeropoint of each WFPC chip as given in the WFPC2 Instrument Handbook (Burrows 1995) varies slightly, photometric offsets were determined for each chip individually. The final magnitudes were calculated from these offsets.

Fields 3 and 5 have overlapping F555W observations and fields 4 and 5 have overlapping F336W observations. This enabled us to make empirical checks on the agreement between measures of the same stars in individual and combined images. The differences in stars of magnitudes to 25 are less than the errors given by ALLSTAR. Thus, we adopt the errors given by the program, which are very similar for individual and combined frames with these exposures and adopted limiting signals.

We made no correction for telescope breathing, although the exposures were short compared with the telescope breathing cycle time. However, the PSF radius and co-addition position limits were large enough that this would be an effect of a few percent or less, and thus not a significant source of photometric error.

Figures 3, 4, and 5 display selected aperture-corrected colour-magnitude diagrams. The magnitudes obtained after this step will be referred to as the *observed magnitudes*. Figure 5 shows error bars for all stars, which are the same as in Figure 3. Figure 4 shows errors bars typical of 3 places in the diagram, as placing errors bars on all stars makes the diagram too crowded to see easily.

4. FOREGROUND CONTAMINATION REMOVAL

Because NGC6822 lies at a low galactic latitude ($b_{1950} = -18^{\circ}40$), and because our fields lie outside the dense central regions of NGC 6822, contamination from foreground Galactic stars is a concern. Wilson (1992) used control fields that were located 30' east and west of NGC6822; this distance would be ideal for this study. A search for WFPC2 images within one degree of NGC6822 was unfruitful; the only objects observed in this region are specific objects within NGC6822 (e.g., OB associations, H II regions). Thus, for decontamination, archival WFPC2 images of the quasar Q1240+1754, taken with the F439W and F675W filters were measured. While they are not ideally placed to match the immediate foreground environment of NGC 6822, they are the only images with some of the same filters and exposures (350 - 400 sec), with suitable CR-split readouts.

The two main fields lie in regions of different light level associated with NGC 6822, and their C-M diagrams also differ in the sense of indicating that the W field contains more NGC 6822 stars. Thus, we also used the NE field as the ‘foreground’ to decontaminate the W field.

To remove foreground stars from the colour-magnitude diagrams of NGC6822, we first established that the limiting magnitude and errors from the photometry were the same, and also compared the total numbers of stars measured in the two fields. The QSO field was less heavily populated, being at higher galactic latitude ($b \approx 80^\circ$), so the density of foreground stars was lower. This was somewhat offset in the overlap fields by their smaller area. In each field being corrected, total numbers of stars were scaled (always upwards) in the control field to match those in the field of interest, at the bright end of the distribution. These comparisons were made with NGC 6822 fields in the NE and W, and were consistent. The scaled QSO field file was increased by adding the same extra fraction of stars in half-magnitude bins, and giving the extra stars magnitudes that differ by 0.01 mag. A script was then written to perform the following: a star in the foreground field is chosen. If there is a star in the background field (the field of interest) such that if

$$\sqrt{\Delta_{color}^2 + \Delta_{magnitude}^2} < x, \quad (1)$$

(where Δ_{color} is the difference in colour between the foreground and background stars, $\Delta_{magnitude}$ is the difference in magnitude between the foreground and background star, and x is an arbitrary fitting radius) then the foreground star cancels out the background star, and both stars are removed, before proceeding to the next comparison.

Because the QSO control field was only observed with filters F439W and F675W, only these colours were used in this exercise. When using the NE fields as control for the W fields, only the relative areas of sky were used in the number scaling.

The results of the foreground decontamination, using a fitting radius $x = 0.1$ mag, are shown in Figures 3 and 5. Our approach to foreground removal is simple, but all that is warranted by the small numbers of stars and photometric errors we have. However, the principal result is the distribution of bright stars in the decontaminated diagrams, and these agree well between the two methods (scaled QSO field and use of NE field), as well as being visible in the uncorrected diagram (Fig 4). Thus, the decontamination process is not critical to the main result we discuss in the next section.

4.1. De-reddening Corrections

The reddening towards NGC6822 has been determined many times in the past, with varying results. Kayser (1967) found, by using two-colour photographic photometry of field stars, a mean foreground reddening of $E(B - V) = 0.27 \pm 0.03$. Hodge (1977) determined that the average value for the reddening towards NGC6822 was $E(B - V) = 0.28 \pm 0.03$. van den Bergh & Humphreys (1979) found $E(B - V) \sim 0.3$ for field stars around the galaxy. Massey *et al.* (1995) showed that there is a spatial dependence of the reddening; reddening is smallest [$E(B - V) \approx 0.26$], on the east and west extremes of the galaxy, and as high as $E(B - V) \approx 0.45$ near the centre. Because the two regions examined in this paper lie well outside the body of the galaxy, we have used a constant reddening value of $E(B - V) = 0.26$ which we regard as almost all foreground. In addition, the ratio $E(U - B)/E(B - V) \approx 0.72$, so a reddening value of $E(U - B) = 0.19$ is used. A distance modulus of 23.49 was used to determine absolute magnitudes.

The dereddening was done after the foreground decontamination, since the reddening of foreground stars will be close to zero in both the NGC 6822 and control fields.

5. RESULTS AND DISCUSSION

In discussing the resulting diagrams we have overplotted the isochrones of Bertelli *et al.* (1994). We find that the isochrones for solar abundance fit the data better than the LMC abundance, although some intermediate value is indicated. We discuss this further below. Figure 5 shows the comparison of models, and for simplicity, only solar abundance models are plotted in Figures 3 and 4. We have converted the model colours from UBVR to the WFPC2 filter passbands, following the WFPC2 handbook. The data are dereddened as above before plotting.

Figures 3, 4, and 5 use the largest dataset that contains the filters illustrated. These do not differ detectably from subsets that overlap in other filters. Because of the large number of images and datasets with overlap, we do not present tables of individual measures. However, the first author will provide tables to those interested.

Comparisons to similar colour-magnitude diagrams for other dwarf irregular galaxies such as Pegasus (Gallagher *et al.* 1998) and Sextans A (Dohm-Palmer *et al.* 1997), and with previous studies of NGC6822 (see e.g., Wilson 1992, Massey *et al.* 1995, & Gallart *et al.* 1996) show two major differences, the most apparent being a relative lack of a main-sequence branch in these new results. This is because the previous studies are in the body of the galaxy, and some targeted specific star-formation regions (OB associations

primarily). Gallart *et al.* (1996) showed that the $[(B - V), V]$ colour-magnitude diagram is useful for studying the youngest stars (ages < 250 Myrs), whereas the $[(V - I), I]$ colour-magnitude diagram contains stars of all ages, up to ≈ 15 Gyrs.

In the outer fields we have observed, there are very few stars, but their age is of interest in establishing their origin and connection with current star-formation. While the numbers are very small, the stars of particular interest are well detected and measured, and thus we feel their implications are worth discussing.

Figure 3 shows the result of using the E field as control for the W field (open circles). This should reveal the difference in populations in the two outer fields, and remove foreground objects. We choose to decontaminate this way as the E field clearly has stars that may be NGC 6822 main sequence which are not present in the W field. As noted, the W field is also closer and within the irregular outer faint flux associated with the galaxy. However, the filled circles are stars in the E field that have no counterpart in the W field.

Figure 4 shows the E and W fields without foreground correction in the two filters with our longest wavelength separation. The same differences in population are seen.

Figure 5 shows both E and W fields combined, corrected by the QSO control field with these two filters.

In all these diagrams, the W field contains a number of brighter blue stars not seen (at all) in the E field, indicating a NGC 6822 population of age some 100 Myr. For Poisson statistics, the excess of main sequence objects in the W field (and the excess of bright red stars in the E field) is significant at $> 3\sigma$ level. The redder population of bright stars in the E field is harder to explain. They are spread over the field, so are not associated with a cluster within NGC 6822. The most luminous stars could be massive NGC 6822 stars in post red giant evolution, whose duration (and hence observed population) is comparable to the main sequence phase. However, the numbers would imply a top-heavy IMF (and small age spread of < 30 Myr), since there are no main sequence stars in this field. Also, there are too few red giant stars (particularly as some might be old metal-poor red giant stars reaching $M_V \sim -2.5$ and $B-V \sim 1.6$), and too many in the region between the main sequence and the red giants at ages around 60 Myr. These stars may also be the giant branch population of stars in our galaxy halo that are unevenly distributed between our E and W fields.

We note that the solar abundance models fit the reddest colours better than the LMC abundance models (see figure 5). In addition, the colours of the bright intermediate stars lie closer to the solar blue loop limit than for LMC abundance. Although, as noted in the previous paragraph, we are not clear what the connection is, overall, the models appear to

fit best for an abundance closer to solar than LMC. While this is not a strong result in view of the small numbers of stars and the outer regions sampled, it differs from the LMC type abundance found in the main galaxy. Thus, the explanation may lie more in understanding the evolutionary status of the red stars than in their abundances.

The bulk of our main sequence NGC 6822 stars, in the W region, are comparable in age with the the oldest stars seen by Gallart *et al.* (1996) in their $[(B - V)_0, M_V]$ colour-magnitude diagram, at about 200 Myrs. To fully examine the older population of the halo of NGC6822, further observations in redder filters (specifically the F814W (*I*) filter) would be needed. The so-called *blue plume* at $(m_{439} - m_{555})_0 = 0$ is composed of both main sequence and blue-loop stars. Gallart *et al.* (1996) were able to differentiate between these two components by noticing a change in stellar density, but because of the low numbers of stars populating the blue plume in this study no such differentiation can be made. The E region shows no sign of a blue plume at $(m_{439} - m_{555})_0 = 0$.

These results may also be compared with the $[(B - V), V]$ colour-magnitude diagram of the Pegasus dwarf irregular galaxy by Gallagher *et al.* (1998), specifically that of the WF3 chip. In the Gallagher *et al.* study, the bulk of the galaxy lay in the PC1, WF2, and WF4 chips, and the WF3 chip contained mostly the outlying regions of this galaxy. The colour-magnitude diagram for this chip shows a very sparsely populated main sequence branch, very similar to what is seen in our diagrams. A main sequence branch is seen in the colour-magnitude diagrams for the other three chips, which is expected, as these chips cover the body of the galaxy.

We suggest that the blue stars seen in the W field represents a younger population that is connected with the streaky faint light seen on the W side of the galaxy, and not seen to the E. Both phenomena may have arisen from a tidal event that disrupted the older population in this direction and also led to the current star-formation activity in the whole galaxy, and also traced in the debris to the W. Wider field imaging with deeper exposures would be needed to explore this possibility further.

We acknowledge the critical reading and helpful suggestions of a referee.

REFERENCES

- Bertelli, G., Bressan, A., Chiosi, C., Fagotto, F., & Nasi, E., 1994, AASuppl, 106, 275
- Burrows, C.J. (Ed.) 1995, Wide Field and Planetary Camera 2 Instrument Handbook (STScI)
- Dohm-Palmer, R.C., Skillman, E.D., Saha, A., Tolstoy, E., Mateo, M., Gallagher, J., Hoessel, J., Chiosi, C., & Dufour, R.J. 1997 AJ, 114, 2514
- Gallagher, J.S., Tolstoy, E., Dohm-Palmer, R., Skillman, E.D., Cole, A.A., Hoessel, J.G., Saha, A., & Mateo, M. 1998, AJ, 115, 1869
- Gallart, C., Aparicio, A., & Vílchez, J.M. 1996, AJ, 112, 1928
- Hodge, P.W. 1977, ApJS, 33, 69
- Hubble, E.P. 1925, ApJ, 62, 409
- Kayser, S.E. 1967, AJ, 72, 134
- Massey, P. 1998, ApJ, 501, 153
- Massey, P., Armandroff, T.E., Pyke, R., Patel, K., & Wilson, C.D. 1995, AJ, 110, 2715
- McAlary, C.W., Madore, B.F., McGonegal, R., McLaren, R.A., & Welch, D.L., 1983, ApJ, 273, 543
- Minniti, D., & Zijlstra, A.A. 1996, ApJL, 467, 13
- Roberts, M.S. 1972, IAU Symposium 44, D.E. Evans (Ed.)
- Stetson, P.B. 1987, PASP, 99, 191
- van den Bergh, S., 1968, Communications of the David Dunlop Observatory, No. 195
- van den Bergh, S. & Humphreys, R.M. 1979, AJ, 84, 604
- Vaucouleurs, G. de, Vaucouleurs, A. de, & Corwin, H.G. 1976, Second Reference Catalogue of Bright Galaxies (University of Texas Press, Austin)
- Wilson, C.D. 1992, AJ, 104, 1374

Captions to figures

Fig. 1.— WFPC2 fields 1 & 2 (the ‘East’ region). The background image comes from the STScI Digitized Sky Survey, and measures approximately $14'.5$ on each side. North is up and E to the left.

Fig. 2.— As in Fig. 1, but for fields 3, 4, & 5 (the ‘West’ region).

Fig. 3.— NGC 6822 W field after foreground subtraction using E field. The filled symbols are stars in the E field that were not matched with any W field stars in the process. Superposed tracks are Bertelli et al (1994) isochrones for ages shown.

Fig. 4.— Widest colour separation plot of stars from overlap regions in E and W fields. No foreground subtraction has been applied. Note the presence of some main sequence stars in the W field.

Fig. 5.— Combined results from E and W fields with foreground subtraction using data with these filters in high latitude QSO field. The presence of NGC 6822 main sequence stars is evident. The solid isochrone tracks are for solar abundance models, and the dashed and dotted ones are for LMC abundance.

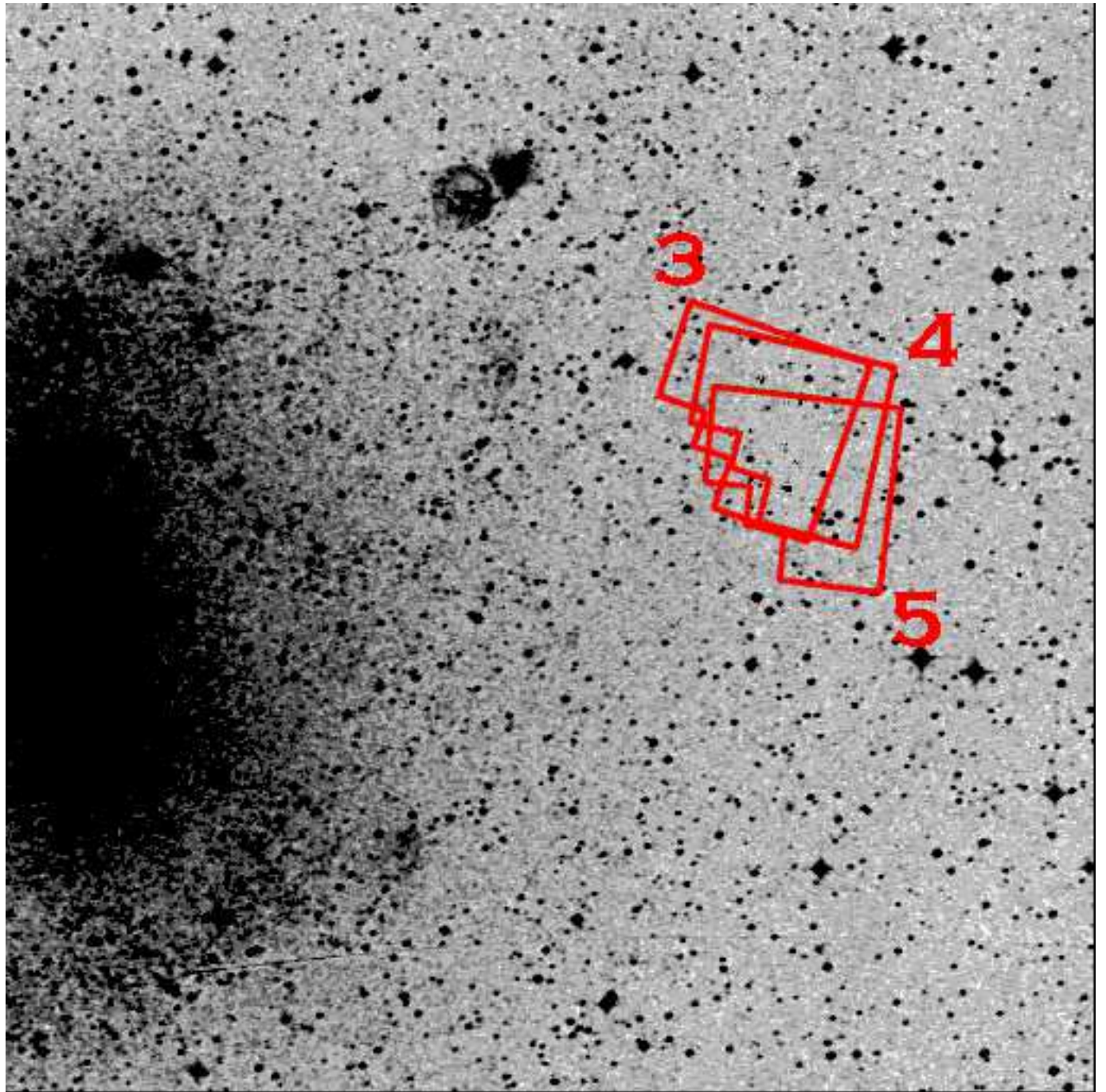
Table 1. Parameters for NGC6822.

		Ref.
α_{2000}	19 ^h 44 ^m 56 ^s .14	
δ_{2000}	−14° 48′ 05″.5	
l_{1950}	25° 34	
b_{1950}	−18° 39	
$(m - M)_0$	23.49 ± 0.08	1
E($B - V$)	0.26	2

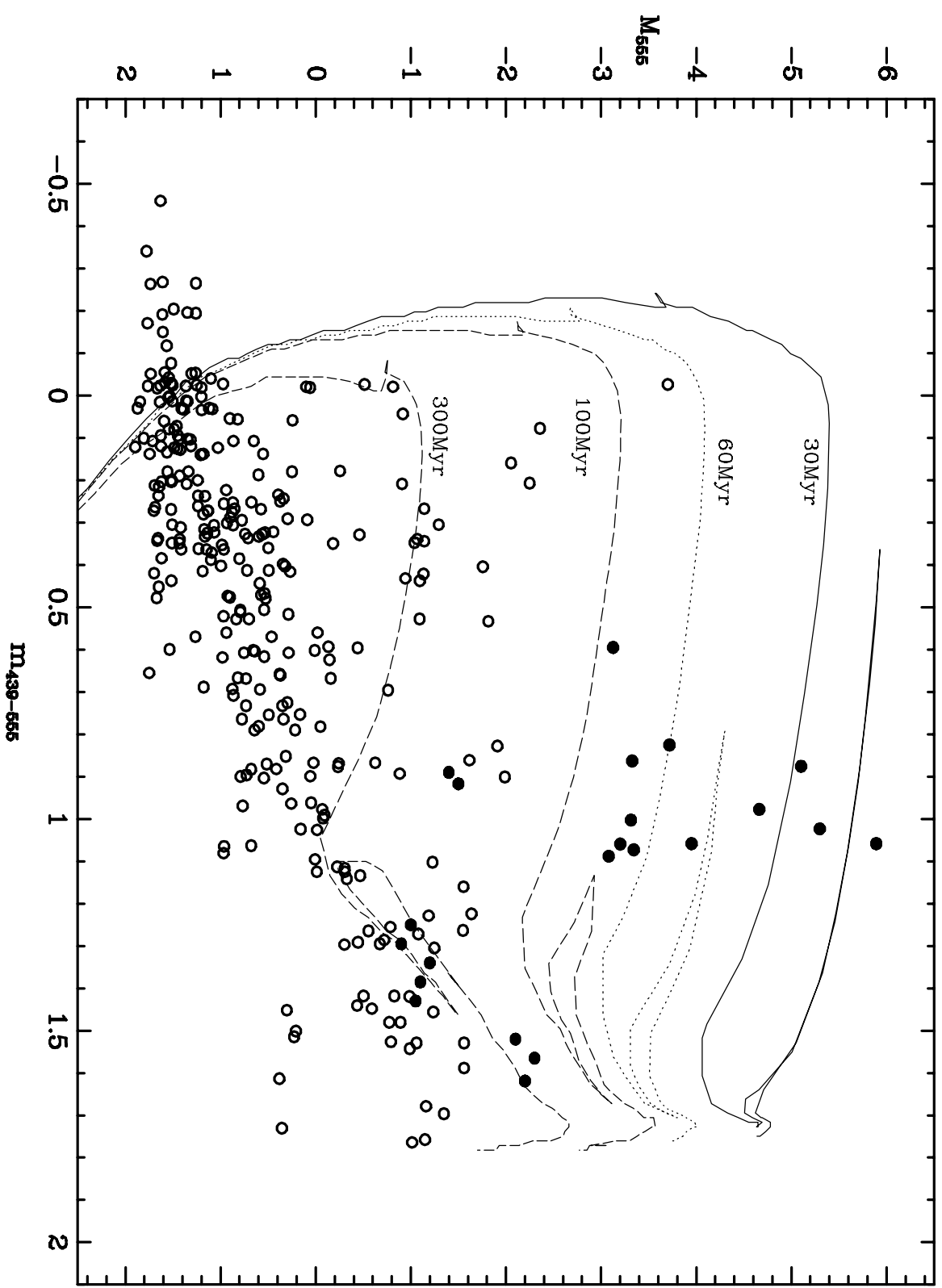
References. — (1) Gallart *et al.* (1996); (2) Massey *et al.* (1995).

Table 2. Journal of observations (GO6567)

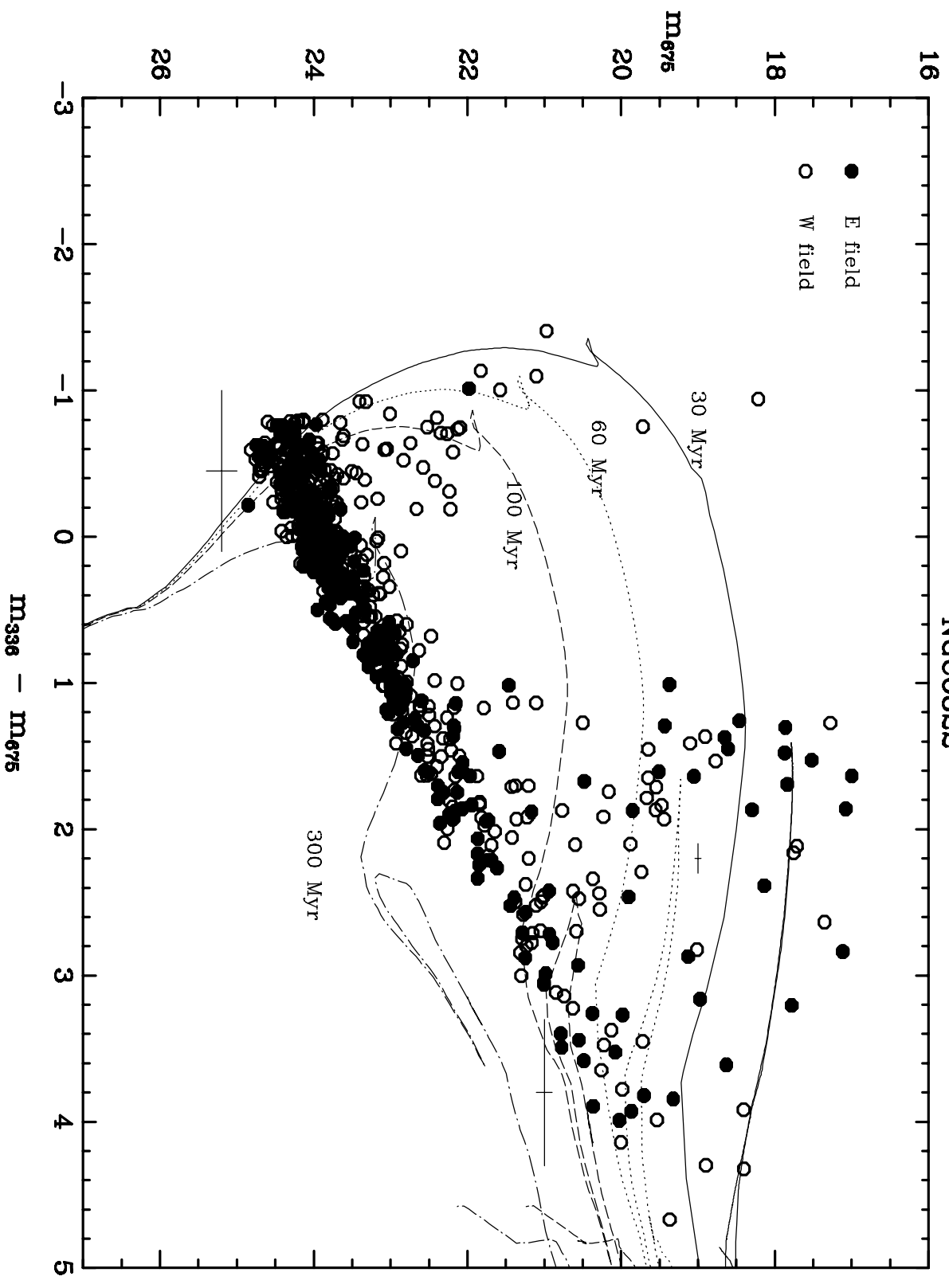
Data set	R.A. (J2000)	Decl. (J2000)	Filter	Exposure time (s)
U3860103T (1)	19 45 36.453	-14 39 14.784	F555W	300
U3860105T (1)	19 45 36.453	-14 39 14.784	F439W	350
U3860203M (2)	19 45 31.972	-14 38 15.956	F675W	300
U3860205M (2)	19 45 31.972	-14 38 15.956	F336W	350
U3860303T (3)	19 44 18.284	-14 45 19.498	F555W	300
U3860305T (3)	19 44 18.284	-14 45 19.498	F439W	350
U3860403T (4)	19 44 16.404	-14 45 32.303	F675W	300
U3860405T (4)	19 44 16.404	-14 45 32.303	F336W	350
U3860503T (5)	19 44 15.706	-14 46 12.936	F555W	300
U3860505T (5)	19 44 15.706	-14 46 12.936	F336W	350



NGC6882 halo



NGC6822



NGC6822 halo-control

